DRD No. SE-5
DRL No. 139

LARGE-AREA SHEET TASK
ADVANCED DENDRITIC WEB GROWTH DEVELOPMENT

C. S. Duncan, R. G. Seidensticker, J. P. McHugh,
R. H. Hopkins, D. Meier, and J. Schruben

Quarterly Report

January 1, 1982 to March 31, 1982
Contract No. 955843
August 18, 1982

The JPL Flat Plate Solar Array Project is sponsored by the U. S. Dept. of Energy and forms part of the Solar Photovoltaic Conversion Program to initiate a major effort toward the development of low-cost solar arrays. This work was performed for the Jet Propulsion Laboratory, California Institute of Technology, by agreement between NASA and DOE.

Westinghouse R&D Center
1310 Beulah Road
Pittsburgh, Pennsylvania 15235

CONTENTS

LIST OF FIGURES

1. SUMMARY

During this quarter, the new "discrete shield" temperature model was completed and verified. Modifications to the J419 low-stress configuration were tested experimentally to evaluate effects on growth speed. A composite lid and shield configuration combining the low-stress features of the J419 with the width-limiting characteristics of the J98M3 was fabricated and tested in the N-furnace. Several long crystals were grown with width limited to about 3.3 cm and with melt replenishment, although the configuration is not yet optimized for steady-state growth.

2. INTRODUCTION

Silicon dendritic web is a single-crystal silicon ribbon material which provides substantial advantages for low-cost manufacture of solar cells. A significant feature of the process is the growth from a melt of silicon without constraining dies, resulting in an oriented single-crystal ribbon having excellent surface features. In common with other more classical processes such as Czochralski growth, impurity rejection into the melt permits the use of less pure "solar grade" starting material without significantly affecting cell performance. A unique property of the dendritic web process is the growth of long ribbons of controllable width and thickness which not only facilitates automation of subsequent processing into solar cells, but also results in high material utilization since cutting and polishing are not required.

On the present contract, three broad areas of work are emphasized:

1. The development of thermal stress models in order to understand the detailed parameters which generate buckling stresses. The model can then be used to guide the design of improved low-stress web growth configurations for experimental testing.

2. Experiments to increase our understanding of the effects of various parameters on the web growth process.

3. The construction of an experimental web growth machine which contains in a single unit all the mechanical and electronic features developed previously so that experiments can be carried out under tightly controlled conditions.

Thus, the principal objective of this work has been to expand our knowledge and understanding of both the theoretical and experimental aspects of the web growth process to provide a solid base for substantial improvements in both area throughput and web crystal quality.

During this reporting period, a new model for calculating the temperature distribution in the growing web was completed. This model can handle any number of discrete lids and top shields and thus permits much more complex configurations to be accurately represented than was possible with the old "lumped shield" model. The model-generated low-stress growth configuration was adapted for melt replenishment and width control and installed in the N-furnace for evaluation.

3. TECHNICAL PROGRESS

3.1 Improved Heat Transfer Model

3.1.1 Introduction

The modeling of the thermal stress and buckling of dendritic web crystals in fact involves three distinct computer codes: 1) a model which calculates the temperature distribution along the growing ribbon; 2) a model which uses the temperature distribution as input and then calculates the thermal stress; and 3) a model which uses the thermal stress distribution as input and then calculates the stability of the ribbon with respect to buckling. With such a sequential type of analysis, it is of obvious importance to have as good as possible a model in the first stage. In fact, the second and third stages of modeling utilize a general, proprietary finite element code, WECAN, which has been shown to be more than sufficiently accurate for our present purposes. The present work concerns the improvement of the calculation of the temperature distribution in the web which forms the basis for the subsequent calculations.

The model which calculates the temperature distribution along the growing silicon ribbon has two distinct routines: a routine which calculates the radiative heat exchange between a point on the ribbon and its environment and a second routine that integrates the heat conduction equation. The problems which occasioned the present work lay not in the integration routine, which had been upgraded earlier, but in the geometrical factors.

For several years, the geometry shown in Figure 1 has been used to evaluate the radiation interchange with the ribbon. This model quite adequately represented the simpler growth configurations used until recently, which had only one or two shields above the lid. Currently,

Dwg. 7768A56

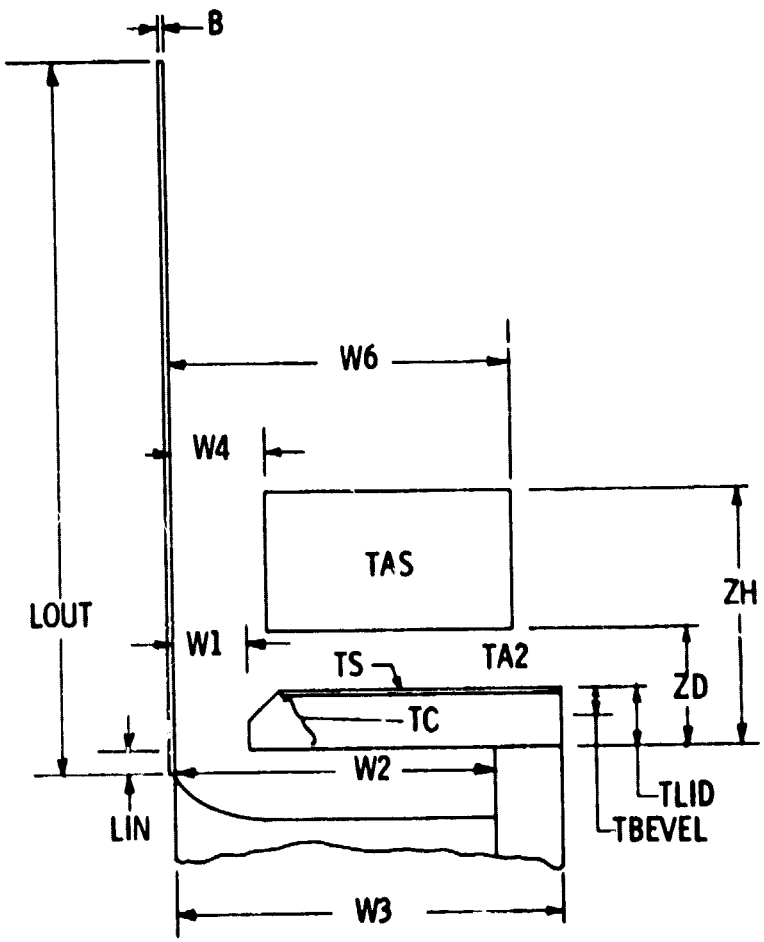

Figure 1. Geometrical and thermal parameters of previous model for calculating temperature profile in the web.

growth configurations with multiple, and occasionally widely spaced, shields are being used, and representation of such a configuration by an isothermal rectangle is suspect. During the reporting period, we have developed a new computer code which allows calculation of the radiative interchange between the web and a number of shields, spacers, etc. so that we have greatly improved the geometric resolution of the model.

As in the previous model, we have neglected other heat transfer mechanisms such as gaseous conduction and convection. Furthermore, we still consider that the absorbance of the silicon ribbon is equal to the emittance, and that the shields, lids, etc. are black bodies so that multiple reflective transfer is neglected. While such refinements might be desired from a theoretical standpoint, the success of the previous modeling suggests that they are second order effects.

3.1.2 Review of Radiative Heat Transfer

Consider the radiative transfer between a single shield at Temperature T_i and an element dx of the web at the point x at temperature T(x) (which is to be determined). Figure 2 illustrates the shield subtending an angle from θ_{i1} to θ_{i2} from the normal to the element dx. The radiative flux density from the shield to the point x on the web is

$$\frac{1}{2}\,\sigma\,T_i^4 \int_{\theta_{i1}}^{\theta_{i2}} \cos\theta\, d\theta \qquad (1)$$

where σ is the Stefan-Boltzman constant. The radiative flux density from the point x to the shield is

$$\frac{1}{2}\,\varepsilon\sigma\,T(x)^4 \int_{\theta_{i1}}^{\theta_{i2}} \cos\theta\, d\theta \qquad (2)$$

where ε is the emissivity of silicon web. Since we are assuming the absorbance of the web equals its emittance, the new flux density transferring from x is

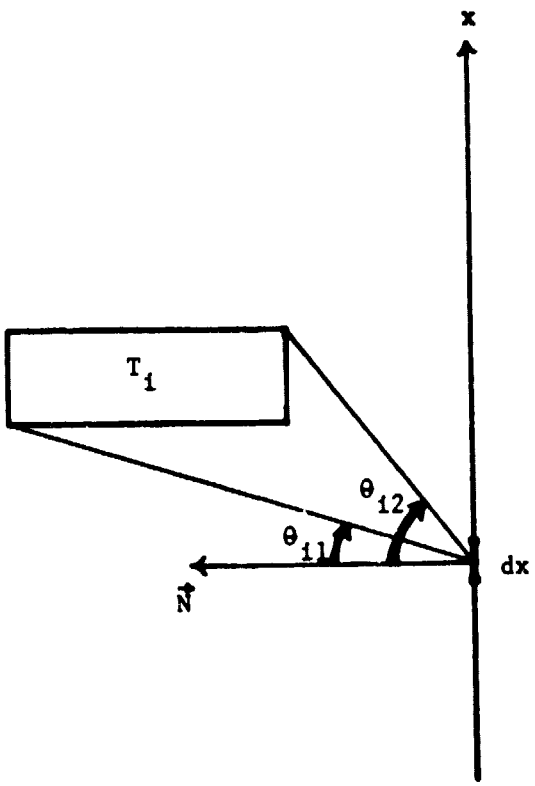

Figure 2. Radiation geometry.

$$q = \varepsilon\sigma\,[T(x)^4 - T_1^4](\sin\theta_{12} - \sin\theta_{11})/2 \qquad (3)$$

The net flux density transfer from any number of elements is the sum of terms like the one above. The essential fact is that once the angular limits and temperature of each element are determined, q may be simply evaluated for substitution in the heat transfer equation[1]:

$$\rho Cu\,\frac{dT}{dx} = \frac{d}{dx}\left(\frac{a}{T}\,\frac{dT}{dx}\right) - \frac{2q}{t} \qquad (4)$$

where ρ = density; C = specific heat; u = pull velocity; a = 318 W/cm, the coefficient of the temperature dependence of thermal conductivity, and t = web thickness. As before, this equation may be integrated to determine the temperature distribution T(x) along the web. We need only evaluate the geometric factors of equation 3.

3.1.3 New Geometry

We examine now the original geometry of Figure 1 to see how it can be systematized for extending its number of elements. A possible systematic arrangement is illustrated in Figure 3; by numbering the ambient regions in sequence with the lid and shields, they may be treated in the same fashion as the other elements. The melt region and the crucible wall are assumed to be at the same temperature and are assigned the number "0". In this case, the ambient region above the top shield would be numbered element 5. The lid is divided into two elements because of the bevel. Since the heat transfer depends only on angular subtense (reflections are neglected), the beveled lid is equivalent to a stepped lid as indicated by the dotted lines. In the previous geometry, the whole lid was isothermal, but now, if desired, different temperatures can be assigned to the top and bottom elements of the lid. In any case, replacing the bevel with a step makes all the elements rectangular in shape. Since the geometries of interest have the back edges of the elements lining up, the ambient spaces can be considered to be comprised of rectangles such as element 3. Thus, the

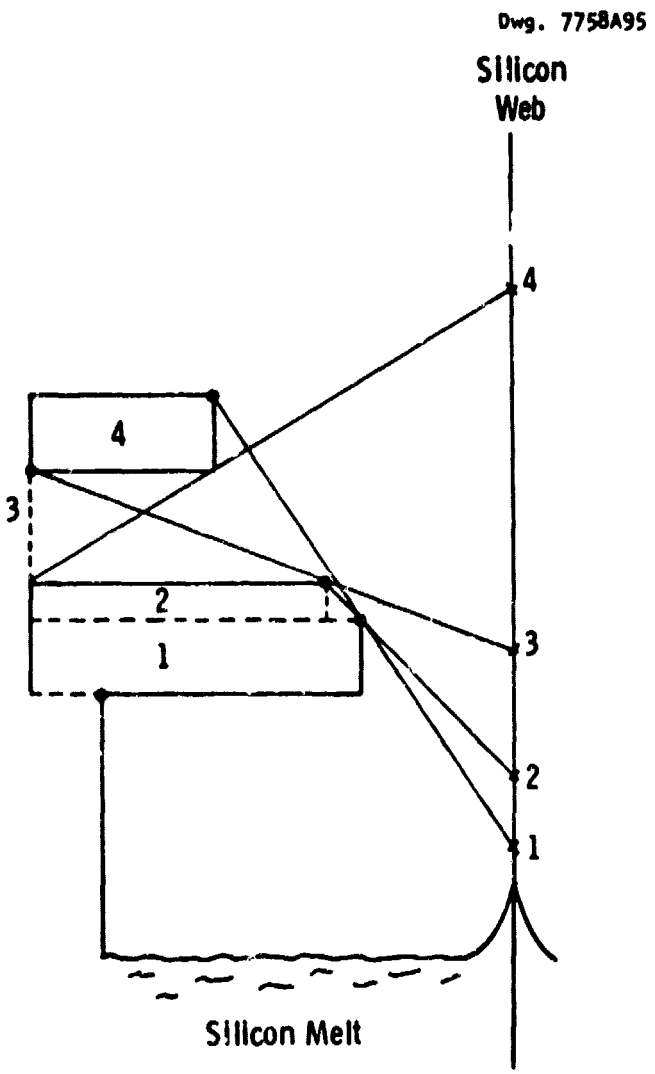

Figure 3. Shading limits for viewing the furnace elements from the web.

geometry is completely determined by the input of the upper corner of each element indicated by the large, black points.

The four numbered points on the web are the boundaries of regions with different views; for example, for points between 3 and 4, all elements are in view, while above 4, the ambient region 3 is invisible. These points along the x-axis can be systematically determined in the following manner. First, the lower "shade" of each element is found by drawing lines through the inner upper corner of each element below it. The highest intersection of these lines on the x-axis is the lower shade. For example, the point 1 is the lower shade of the 4th element; element 4 is invisible for points on the web below point 1.

After all the lower shades are found (some elements may not have any), then the upper shades are found. The lower inner corner of an element is connected to the lower inner corner of each element above it. The lowest intersection point of each of these lines with the x-axis is the upper shade of the element in question. For example, element 2 does not have an upper shade, while element 3's upper shade is the point 4 on the web; element 3 is invisible above point 4 on the web.

After all the upper and lower shades are found, these points are ordered on the x-axis. The region between two such points is assigned a vector, the ith component of which is either one or zero depending on whether or not the ith element is visible to points in this region.

Figure 4 illustrates a possible geometric configuration for the new model. Numerical integration of the heat conduction equation proceeds up the silicon web from the melt surface. By knowing in which region between upper and lower shades the point of integration lies, we know which elements are visible to it. For the point illustrated, elements 0 (the melt), 4, 6, 7, 8, and 15 (ambient) are visible. There is one additional piece of information needed before the integration can proceed: the element opposite the point of integration, element 7 in this case. For the visible elements numbered 7 or less, the lower inner corners are used to limit the viewing angles while for elements 7 or

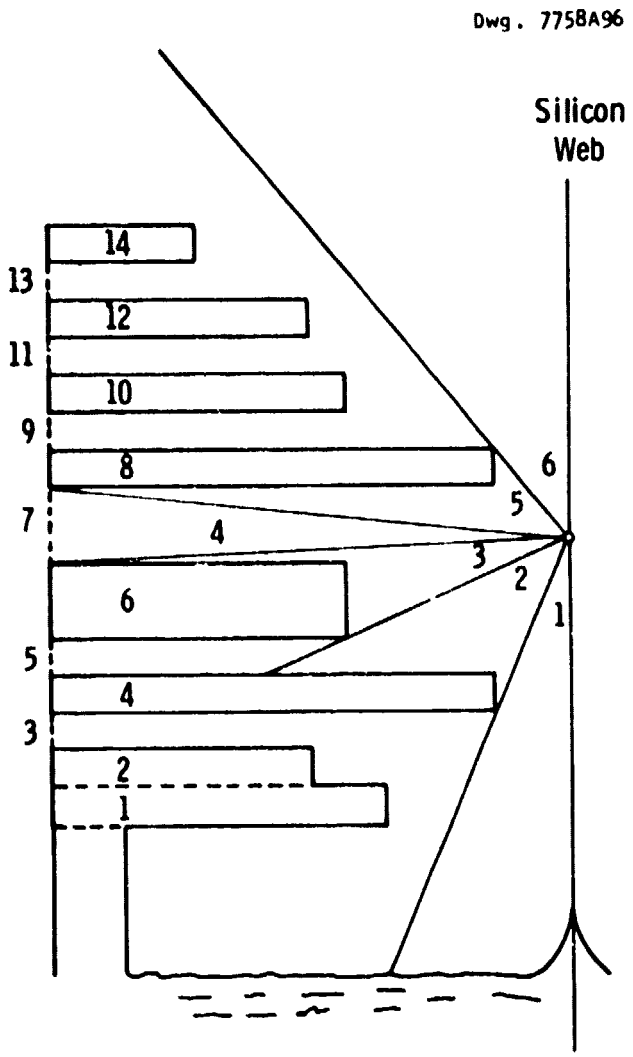

Figure 4. Viewing regions from a point on the web.

greater, the upper inner corners are used as illustrated. The viewing regions are labeled 1 through 6; these determine the proper coefficient q of the heat conduction equation during integration.

Once the geometrical heat transfer coefficients have been calculated, equation 4 can be numerically integrated to yield the temperature distribution along the length of the web crystal. A more detailed description of the computer code will be presented in a future report.

3.1.4 Verification of the New Model

One of the modeling runs of the J419 configuration, Case 9-11C, was used to verify the new radiation transfer model. The first test was to run the identical configuration, i.e., a lumped shield model as in Figure 1, to verify the operation of the routine which evaluates the shade points, etc. The results were excellent; the new program gave the identical temperature profile as the older program. A second geometry was then evaluated in which both the lid and the shield "block" were beveled. This is a relatively small change in the geometry, but one that could not be accommodated by the older model. It would be expected that the results be similar, but not identical, and that was indeed the case.

Figures 5 and 6 illustrate the two cases.* However, instead of presenting the temperature profiles themselves, the figures show the second derivative of temperature times thermal expansion coefficient, i.e., $(\alpha T)''$. This parameter was chosen because it accentuates the curvature of the temperature which can basically be considered as the cause of thermal stress. Examination of the two figures shows that indeed the two profiles are almost the same, although there are some slight differences due to the more complicated profile.

*These figures were generated by a computer plotting routine which has been added to the temperature distribution model. Not only is $(\alpha T)''$ plotted, but also the lid and shield geometry is represented (heavy lines in the figures).

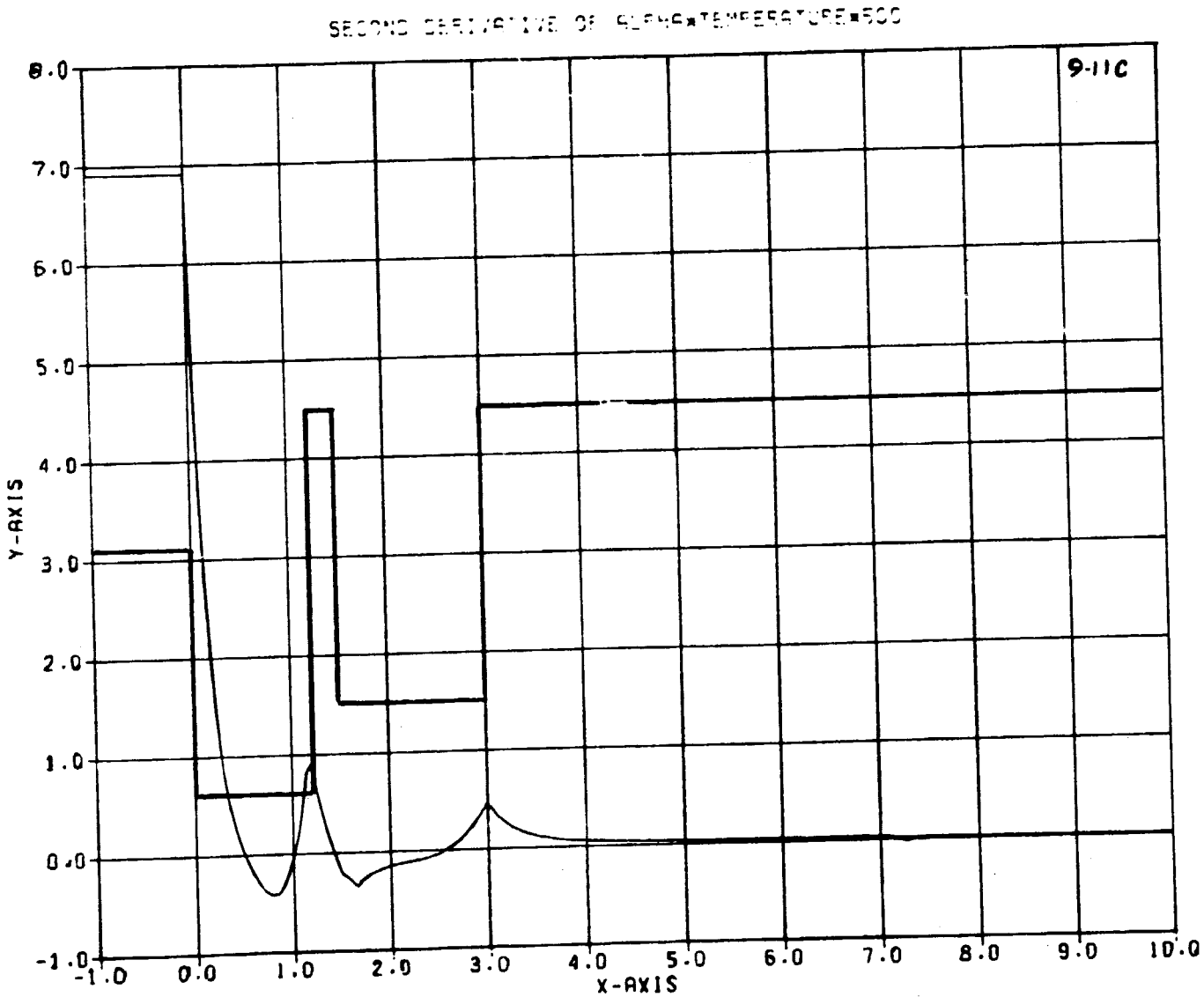

Figure 5. Model geometry and (αT)" for run 9-11C.

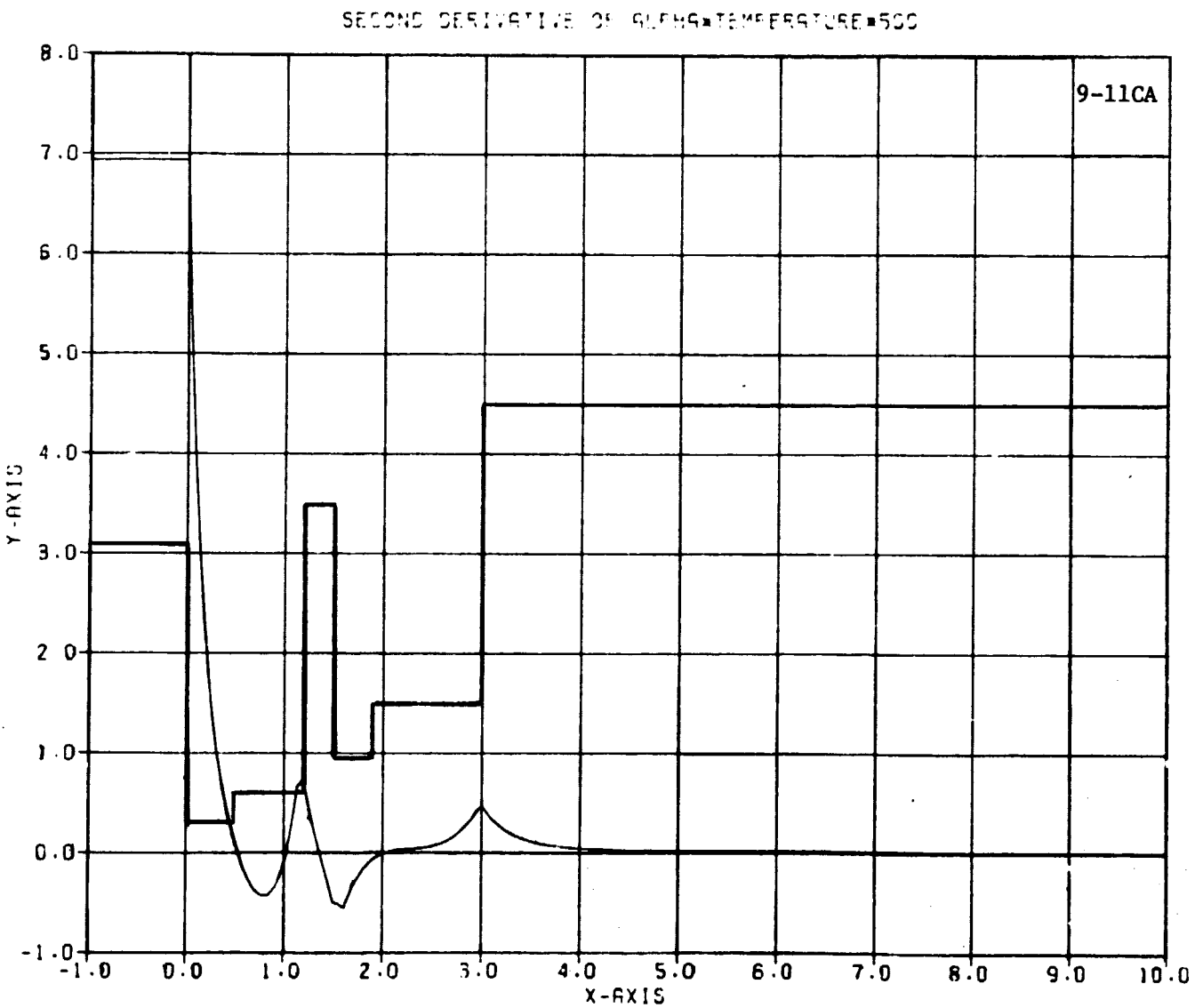

Figure 6. Model geometry and $(\alpha T)''$ for run 9-11CA (beveled elements).

3.2 Growth Experiments

During the early part of this reporting period, growth runs in the new experimental facility (N-Furnace) were dedicated to achieving the proper furnace adjustments for continuous feeding of a standard width-limiting J98M3A lid and shield assembly combined with an elongated crucible. Previous runs had indicated that when the adjustable end shield position was proper for melting the feed pellets, then the melt profile was too dipped (colder in the center of the growth slot than at the ends), which led to growth instability, pull outs, and extra dendrite generation. Increasing the diameter of the outboard end holes in the lid flattened out the melt profile and greatly improved the general growth.

Although the melt level control system components all functioned, it became apparent that the system as a whole was not properly tuned to the growth requirements. Several changes were made in the control loop which brought the response time and loop gain into better agreement with the control requirements, and excellent results were then obtained with actual web growth. In one run, several crystals were grown under automatic level control. During the whole course of the run, all the crystals maintained a constant thickness within about 4 μm (at one constant growth speed) and even the hold temperature did not change by more than a few microvolts. The extreme stability of the growth conditions would indicate that the level control system was operating even better than required!

The modifications made to the N-furnace melt level control system to better meet growth requirements were three in number. First, the time constant of the control loop was made adjustable so that integration periods of 1, 20, 100, and 400 seconds could be used. The faster response times are used for the initial set up of the equipment, but the longer times are needed to avoid unnecessary fluctuations in the final feed rates. With the longer integration times, a higher loop gain can also be used and the response gain of the sensing circuit was

increased by a factor of about ten. As a result, the control capabilities of the system are easily of the order of 100 μm or better in melt height sensing. Finally, a selectable limiting speed was placed on the pellet feed motor in order to prevent overfeeding during transient conditions.

Several modifications of the computer model-generated J419 configuration were tested in the J-furnace in an effort to enhance the growth speed of this wide-growth, low-stress design. In one series of experiments, the J419 was modified to a more open geometry by beveling the top lid and using a different shield stack order. The expected speed enhancement occurred, as did a change in the residual stress character. Whereas the standard J419 configuration produced crystals with negative residual stress, the modified version gave material with positive residual stress. In both cases, the magnitude could be either very small or moderate, depending on other growth parameters. The higher speed modifications also would grow moderately wide material, up to 40 mm, but tended to deform at slightly narrower widths than the unmodified J419.

The earlier modeling results suggested that the residual stress in some of the higher speed versions of the configuration could be reduced by reducing the heat loss from the web in the interface region. One feature of a lid design which would accomplish this would be a bevel on the bottom edge of the slot in the lid. Thermally, this would allow the web to "see" the hot crucible cavity for a greater portion of its length so that the heat loss near the growth front would be decreased.

Four runs (J439-J442) were made in which the top lid was either unbeveled or had a 3 mm bevel; the bottom lid had either a 1.5 mm or a 3 mm bevel. It was found that the bevel on the bottom of the lid had more effect on speed than on residual stress, while the bevel on the top lid affected the stress more than the speed. Although the previous thermal model does not have enough resolution to evaluate these effects, the new model should easily accommodate these geometry changes and will be used to provide the required insight into the behavior of the system.

While modifications to the J419 configuration were being tested in the J-furnace, experiments in the WA-furnace were directed to testing the compatibility of the J419 configuration with the elongated crucible which would be required for growth at constant melt level. Adjustable end shields were installed. Melt probe data showed that the lateral coil position and the end shield height affect the melt profile differently and that adjustment of both parameters is necessary to obtain a flat, symmetric temperature distribution in the melt. However, when the proper melt temperature profile was achieved, it was established that the low-stress characteristics of the J419 configuration were maintained with the elongated crucible configuration.

At this point it seemed appropriate to combine the wide-growth, low-stress capabilities of the J419 configuration with the width-limiting behavior of the J98M3A configuration for demonstrating extended growth runs. Lids and shields were fabricated which combined these features in a hybrid configuration now known as the J435. Four runs were made with this configuration in the J-Furnace to evaluate the width-limiting capabilities of the design, and the results confirmed a steady growth width between 28 mm and 33 mm, depending on the furnace parameters.

Feed holes and laser holes were then added to the J435 lids and shields and the hardware installed in the N-Furnace with an elongated crucible for melt replenishment. Preliminary experiments focused on optimizing the end shield adjustment and the work coil position so that the melt profile is compatible with both steady-state width and melt replenishment.

Several growth runs were made both with and without melt replenishment. In one run, a 4.8 meter crystal was grown with the width held at 3.1 to 3.3 cm for 3.4 meters. This crystal was grown without replenishment due to clogging of the feed hole with oxide. Several shorter crystals were grown with replenishment, with thickness constant to within a few microns and width limited in the 3.1 to 3.3 cm range.

We found that clogging of the feed hole with oxide can be prevented by constantly feeding pellets at a slow rate throughout the run, whether a crystal is growing or not. We will also test some modifications in the feed hole geometry to alleviate this problem.

4. CONCLUSIONS

The new temperature model will allow complex lid and shield configurations to be evaluated for stress-inducing characteristics with the computer. The greatly improved resolution also permits minor design variations to be tested so that only the most promising designs need be fabricated into hardware for experimental evaluation. Thus, the experimental effort can be concentrated on designs with high probability of success and on refinements which can only be tested empirically.

The J435 configuration, which combines the stress-reducing characteristics of the J419 with the width-limiting capabilities of the J98M3, has been tested in the N-furnace and appears capable of producing long crystals about 3.3 cm in width. Further refinements are needed to better control oxide deposition, and the optimum melt level for steady-state growth is yet to be determined.

5. PLANS AND FUTURE WORK

The new temperature model will be used to generate new lower stress growth configurations. Experimental work will continue to optimize the J435 configuration for steady-state growth.

6. NEW TECHNOLOGY

No new technology is reportable for the period covered.

7. REFERENCE

1. C. S. Duncan et al., Silicon Web Process Development--Annual Report, May 31, 1978. DOE/JPL 954654-78/1. p. 195.

8. ACKNOWLEDGEMENTS

We would like to thank H. C. Foust, E. P. A. Metz, L. G. Stampahar, S. Edlis, W. B. Stickel, and W. Chalmers for their contributions to the web growth studies.

9. PROGRAM SCHEDULE COSTS

9.1 Updated Program Plan

9.1.1 Milestone Chart (see page 24)

9.1.2 Program Cost Summary (see page 25)

9.1.3 Program Labor Summary (see page 26)

9.2 Man-Hours and Costs

Man-Hours		Costs	
Previous	18,566	Previous	$1,024,522
This Period	9,116	This Period	197,555
Cumulative	27,682	Cumulative	1,232,077

LSA PROJECT
LARGE AREA SILICON SHEET
ADVANCED DENDRITIC WEB GROWTH DEVELOPMENT
MILESTONE CHART – JPL CONTRACT 955843